Statistical Analysis of the Surface Circulation in the California Current System Using Satellite-Tracked Drifters

PIERRE-MARIE POULAIN AND PEARN P. NIILER

Scripps Institution of Oceanography, La Jolla, California

(Manuscript received 8 December 1988, in final form 4 May 1989)

ABSTRACT

A kinematic description of the surface circulation in the southern California Current System is presented using the statistics of the 7–11 month long trajectories of 29 satellite-tracked mixed layer drifters. The drifters were released north of 30°N and traveled southward at an average speed of 3–4 cm s^{-1} along Baja California through an inhomogeneous field of mesoscale eddies of 15 cm s^{-1} rms variability. Lagrangian and Eulerian statistics of the variations about this mean southward drift are computed. The drifter ensemble mean Lagrangian decorrelation time scale is 4–5 days and the Lagrangian decorrelation space scale is 40–50 km. The computation of dispersion of single particles about the mean drift shows that the theory of diffusion by homogeneous random motion (Taylor's theory) describes these dispersive motions well. Ensemble mean diffusivities of about 4×10^7 cm^2 s^{-1} are found. On a 200 × 200 km^2 spatial average, single-partial diffusivities are found to be proportional to the kinetic energy of the locally inhomogeneous fluctuations. Particle-pair statistics are used to study the relative dispersion of particles. The relative diffusivities depend on the initial separation and on the duration of drift. The results are compared to Richardson's ⁴⁄₃ power law. The Eulerian spatial and temporal correlation of the velocity field indicates that the eddy field is isotropic for scales less than 200 km. The zero time lag correlation indicates an Eulerian length scale of 80 km. The 25-day lagged correlation function indicates that a 2 cm s^{-1} northwestward propagation of features exists roughly perpendicular to the mean flow.

1. Introduction

The use of freely drifting objects for measuring current systems has become increasingly common during the last decade. Ocean surface currents roughly estimated in the past from the drift of ships, bottles, cards, etc. can now be measured by calibrated drifters remotely tracked by radio or satellite. Drifter trajectories provide a rich description of the oceanic circulation over a broad range of scales including large-scale flows and mesoscale eddy fields. Perhaps the most extensive descriptions of circulation using drifters in the North Pacific are the observations of the near-surface circulation in the North Pacific westward drift from the trajectories of satellite-tracked drifters (McNally et al. 1983) and the Lagrangian analysis of the circulation on the continental shelf off northern California by Davis (1985a,b). We here discuss the first large scale drift measurements made in the California Current System (CCS).

Besides ship drifts, the first reported Lagrangian measurements of currents in the North Pacific eastern boundary current or CCS date back to the late 1930s. Drift bottles and cards were launched during hydrographic cruises and a coarse estimate of current could be made from the recovered drifters. (Tibby 1939;

Schwartzlose 1963). Also, clusters of drifters tracked by radar from the ship for a few days, have been used to describe mesoscale features of the CCS (Jennings and Schwartzlose 1960; Reid et al. 1963).

Our description of the surface circulation is based on 29 satellite-tracked drifters deployed in 1985 and 1986 off the Southern California and Baja California coasts. The drifters meandered south and revealed a complex and intense mesoscale activity of the surface circulation. This paper presents a statistical kinematic analysis of their tortuous motion. The drifter configuration, the drifter dataset and its basic statistics are presented in section 2. Spatial variations of the velocity field are also discussed. Lagrangian statistics which are presented in section 3 lead to a description of absolute (single-particle) and relative (two-particle) dispersion of particles by the eddy field. Section 4 contains Eulerian statistics inferred from the drifter tracks. The essential results of our statistical calculations are discussed and synthesized in section 5.

2. The drifter data and its basic statistics

Two sets of drifters drogued at a nominal depth of 14.8 m, were released in the CCS in 1985 and 1986. The drifter configuration was of TRISTAR-I in 1985 and of TRISTAR-II in 1986 (Niiler et al. 1987). The question of whether the drogue remained attached to the surface buoy was investigated by recovering one

---

Corresponding author address: Dr. Pierre-Marie Poulain, Scripps Institution of Oceanography, Mail Code A-030, La Jolla, CA 92093.

drifter 4 months after deployment and a second drifter 8 months after deployment. No mechanical wear was evident, although some gooseneck barnacles had grown on the tether line. This first set of drifters were designed very conservatively and, by comparing tracks with later releases in 1987 when we know that drogues fell off because thermistor cables parted, it is apparent all of these drifters have intact drogues.

Niiler et al. (1987) discuss the drifter design and water following capabilities in the mixed layer. For the wind-wave conditions in the CCS in July 85, they measured a slip of TRISTAR-I's with respect to the water of about 2 cm s^{-1}. TRISTAR-II's were designed to reduce this slip by a factor of two. In this environment, the slip relative to the water is primarily caused by the wind. Climatological winds in the vicinity of 31°N, 119°W (x_1 = 300 km and x_2 = −100 km in Fig. 1) are from the northwest and the monthly wind speed averages 6.3 m s^{-1} (Nelson 1976). According to Niiler et al. (1987), these winds can produce a slip of 2 cm s^{-1}. Because of this unavoidable slip, the drifters are regarded as quasi-Lagrangian particles. Although called mixed layer drifters, the TRISTAR's sample the average flow between 13 and 17 m (TRISTAR-I) or between 12 and 18 m (TRISTAR-II). In summer, the

vertical thermal structure of the upper ocean in the CCS can be very complex and there can be very shallow (<10 m) mixed layers (Haury et al. 1986). In that case, the drifters follow the water in the upper seasonal thermocline. In winter, the upper mixed layer is deeper and the drifters are more likely to sample the circulation in the mixed layer.

The drifters were tracked by satellite by means of the ARGOS system. Position fixes averaged five per day. Position accuracies were estimated from time series of three drifters which were apparently stolen and continued to broadcast for a few weeks from some seafarers' collection of flotsam. Location errors have a small decorrelation time (<0.1 day) and have root mean square (rms) values of 200 and 300 m for the meridional and zonal directions, respectively. Velocities were computed from pairs of positions and were assigned the position and time midway between the two observations. The histogram of time intervals between consecutive fixes is strongly peaked at 0.08 day. Using this value and the above position errors, we estimated an rms velocity error of 4 and 6 cm s^{-1} for the meridional and zonal directions, respectively. For the calculations presented in this paper, position and velocity time series were linearly interpolated at 0.2
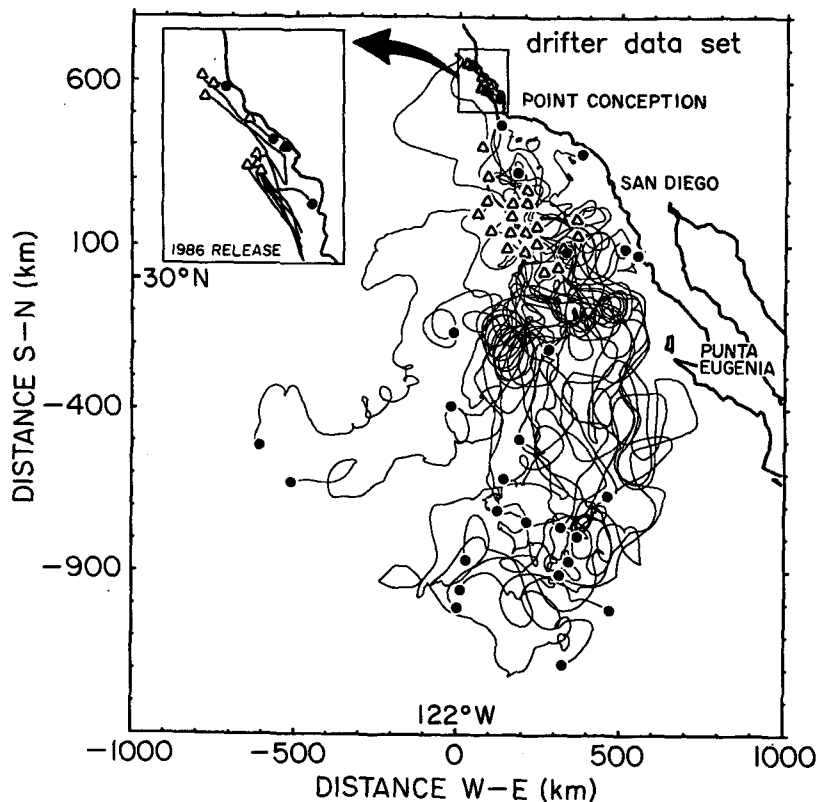

FIG. 1. Position diagram of the 1985 and 1986 drifter data. The trajectories have been low-pass filtered (3-day running mean). Triangle and solid circle symbols indicate sites of first and last observations for each drifter.

day intervals and a 3-day running mean filter was applied to remove small scale/high frequency movements, especially the energetic diurnal/inertial component. This low-pass filter reduces the rms velocity errors to a value less than 2 cm s^{-1}.

A position diagram of the smoothed tracks of both 1985 and 1986 drifters is presented in Fig. 1. The first set of 20 drifters was released during Leg I of the FRONTS cruise in July 1985 (Haury et al. 1986). They were deployed in a persistent, seasonally-recurring front in the CCS southwest of San Diego, California (Niiler et al. 1989). The second set of nine drifters was deployed in March 1986 during the SQ86 cruise along the central California coast about 100 km north of Point Conception (Hayward et al. 1987). The drifters have an average lifetime of 9 ± 2 months (Poulain et al. 1987). Throughout this paper, drifter positions and velocities are given with respect to a Cartesian coordinate system aligned with the zonal (west–east; subscript 1) and meridional (south–north; subscript 2) directions.

The averaged velocity from the global dataset (29 drifters, 5844 drifter-days) is $\langle \mathbf{u} \rangle = \langle (u_1, u_2) \rangle = (0.3, -3.8)$ cm s^{-1}. Variances about that mean were computed, $\langle u_1' u_1' \rangle = 103.2$, $\langle u_2' u_2' \rangle = 118.9$, $\langle u_1' u_2' \rangle = -1.4$ cm^2 s^{-2}, giving an rms speed of about 15 cm s^{-1}. Velocity distributions are approximately Gaussian and the Student t-test was used to find confidence intervals. It will be shown later that the drifters have a

FIG. 3. Spatial distribution of the mean surface flow. Squares with more than 50 drifter-days and with more than 2 different tracks are contoured by a solid line.

Lagrangian integral time scale of about 5 days, and an Eulerian space scale of less than 100 km. We binned the space–time domain using these scales and counted the number of bins containing observations from different drifters. Thus, we found that the number of statistically independent observations is about 1000 and that the 95% confidence intervals on the velocity averages are (0.6, 0.7) cm s^{-1}. The southward mean velocity of the drifters is a significant signature of the mean California Current. It must be kept in mind, however, that about 2 cm s^{-1} of the southward flow can be ascribed to the wind-produced slip. The space and time mean California Current in this region is a very weak circulation indeed. No zonal drift is found at the 95% confidence level. Zonal and meridional variances have the same value at the 95% confidence level.

In order to explore the large-scale spatial variability of the field, we assumed stationary statistics. Drifter velocities were averaged in spatial bins of 200 × 200 km^2 (Fig. 3). This mean circulation must be interpreted with great caution since the number and the time span of observations (Fig. 2) may vary substantially from one square to another. Squares with large means have very little data as drifters do not spend very much time there. Let us focus our attention to the squares which contain more than 50 drifter-days and more than 2 different tracks (contoured by a solid line in Fig. 3). This distinction is rather arbitrary and is made for the sole purpose of separating squares with many observations from others with only a few data points. Despite the fluctuations due to the nonuniform sampling, we see that the mean currents are essentially
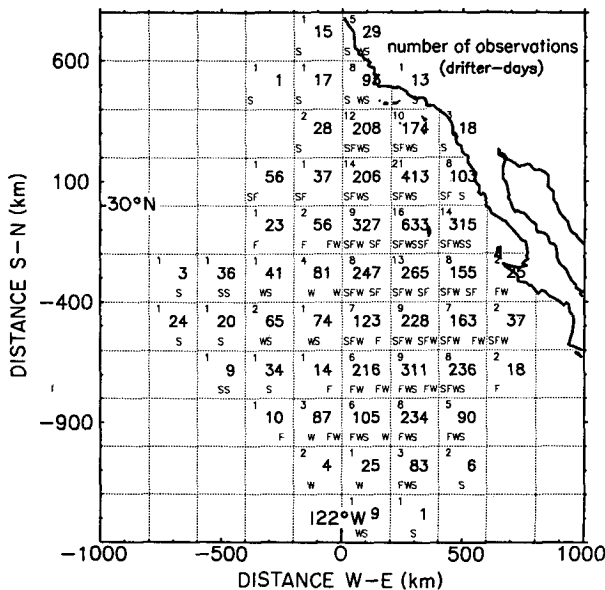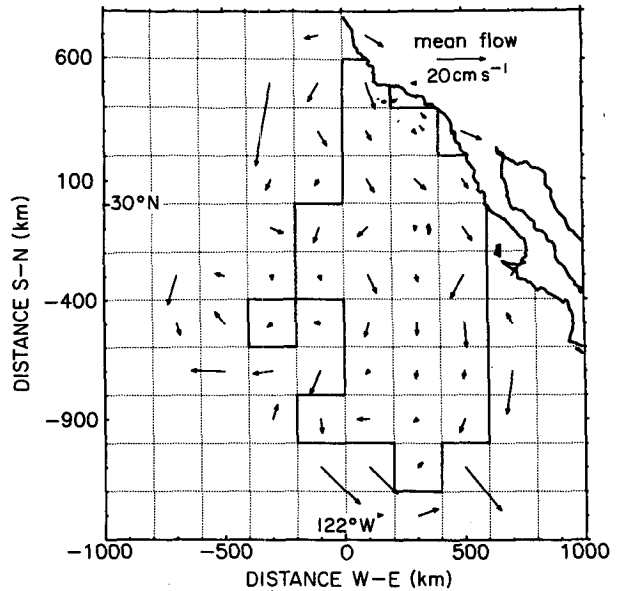

FIG. 2. Spatio-temporal distribution of the drifter data. The number centered in each square represents the number of observations in drifter-days within that 200 × 200 km^2 bin. Time is annotated by the first letter of each season. From left to right, the seasons are summer and fall 85, winter, spring, summer and fall 86, and winter 87. The number of different drifter tracks is posted in the upper left hand corner of the squares.

southeastward north of $x_2 = 0$ km, southward between $x_2 = 0$ and $x_2 = -600$ km, and southwestward south of $x_2 = -600$ km. This picture is compatible with the classic geostrophic surface circulation in the CCS (Reid 1988). The very small mean currents around $x_1 = 300$ km and $x_2 = -200$ km are due to the presence of large (100–150 km) and persistent (2–3 months) cyclonic eddies. These vortices seem to be shed off Punta Eugenia and move northwestward counter to the mean flow. They entrap drifters for many months (12 of 29 drifters circuited at least once around such eddies) and appear to be a barrier to the southward flow of particles. In contrast, a substantial southward flow appears to the east and west of that location.

The residual velocities about that mean circulation have an average rms value of 15 cm s^{-1}. The corresponding principal axes of variance (cf. Freeland et al. 1975) have significant variations (Fig. 4). They decrease from two maxima within 500 km off the coast and south of $x_2 = -800$ km to a minimum centered at $x_1 = 200$ km and $x_2 = -600$ km. Wherever the variance shows significant anisotropy, energies appear to be larger in the meridional direction.

3. Lagrangian statistics and diffusive transports

The quasi-Lagrangian nature of the drifter tracks is exploited to obtain Lagrangian scales of variability and to describe diffusive transports by the eddy field. First, Lagrangian scales of variability from individual drifters are briefly discussed. Second, single-particle statistics are calculated and the theory of diffusion by homogeneous turbulence is tested. Third, the spatial vari-

ability of the diffusivities and their connection to the kinetic energies are studied. Last, relative dispersion is investigated using particle-pair statistics.

a. Lagrangian scales of variability from individual drifters

Let $u(x_0, t)$ be the velocity at time t of the drifter passing through x_0 at the initial time t_0. The Lagrangian autocovariance is generally defined as

$$R_{ij}(\tau, T, t_0, x_0) = \frac{1}{T} \int_{t_0}^{t_0+T} u_i'(x_0, t)u_j'(x_0, t + \tau)dt$$

$$= \langle u_i'(x_0, t)u_i'(x_0, t + \tau) \rangle_L, \quad (1)$$

where $u'(x_0, t)$ is a residual velocity and

$$\langle \quad \rangle_L = \frac{1}{T} \int_{t_0}^{t_0+T} dt$$

is a Lagrangian average. For homogeneous and stationary fields, the dependence on T, x_0 and t_0 vanishes.

Residual velocities are defined by removing the mean velocity for each drifter, $u' = u - \langle u \rangle_L$. The components of the Lagrangian autocovariances from individual drifters are presented in Poulain et al. (1987). There is a great deal of variability in the individual autocovariance functions. Most of these have significant negative lobes and approach a nonzero value at large time lag.

The Lagrangian integral time and space scales are the time and the distance over which a drifter remembers its path. They are defined by

$$T_i^L \equiv \frac{1}{\langle u_i'^2 \rangle_L} \int_0^t R_{ii}(\tau)d\tau \qquad (2)$$

$$L_i^L \equiv \frac{1}{[\langle u_i'^2 \rangle_L]^{1/2}} \int_0^t R_{ii}(\tau)d\tau = [\langle u_i'^2 \rangle_L]^{1/2}T_i^L. \quad (3)$$

The integral of the autocovariance which appears in these definitions [and also in the definition of the diffusivity (5)] is generally time dependent and does not approach a constant limit as t increases. Throughout this paper, we adopt the usual practice of integrating from zero to the time of the first zero crossing. This corresponds to the first maximum of the integral scales and the values can be considered as upper bounds to the true scales.

Four drifters with very small lifetimes (≤ 12 days) were discarded for the calculation of the Lagrangian statistics presented in this section. The statistics of the time and space scales computed from the individual drifters are presented in Table 1. Standard deviations appear larger in the meridional direction. The Lagrangian autocovariances of drifters 08 and 04 are plotted in Fig. 5 to illustrate the scale variations. Drifter 08 was captured by an equatorward-flowing "river" and has meridional time and length scales of 14 days and 120 km. In contrast, the trajectory of drifter 04 is more
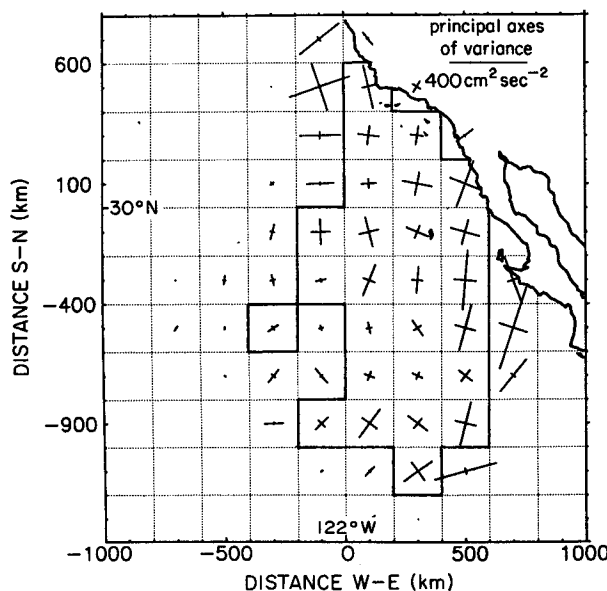
FIG. 4. Principal axes of the variance tensor defined with respect to the mean flow displayed in Fig. 3.

TABLE 1. Lagrangian scales and diffusivities (mean and standard deviation) from individual drifters.

	Time scale (days)		Length scale (km)		Diffusivity K (10^7 cm^2 s^{-1})	
	Zonal	Meridional	Zonal	Meridional	Zonal	Meridional
25 drifters	4.6 ± 1.3	6.1 ± 3.4	39. ± 13.	54. ± 28.	4.1 ± 1.8	5.9 ± 3.7

like a random walk with much smaller integral scales (T_2^L = 3 days, L_2^L = 20 km). This scale variability reflects the inhomogeneous and nonstationary coherent flow structures characterizing the surface circulation in the CCS.

b. Single-particle dispersion

The probability density of particle displacements $P_1(\mathbf{x}, t; \mathbf{x}_0, t_0)$ plays a major role in the transport of the mean concentration of a passive scalar property θ (Davis 1983). Its second moment is the displacement covariance and is defined as

$$\langle d'_i d'_j \rangle(t) = \int P_1(\mathbf{x}, t; \mathbf{x}_0, t_0) d'_i d'_j d\mathbf{x}, \qquad (4)$$

where $\mathbf{d}' = \mathbf{x} - \mathbf{x}_0 - \langle \mathbf{u} \rangle(t - t_0)$ is a residual displacement, $P_1(\mathbf{x}, t; \mathbf{x}_0, t_0)$ is the probability that a particle released at ($\mathbf{x}_0, t_0$) reaches ($\mathbf{x}, t$) and the integration is over the whole space.

For homogeneous and stationary fields, a simple formula relates the single-particle or absolute diffusivity

FIG. 5. Zonal (solid) and meridional (dashed) Lagrangian autocovariances versus time lag for drifters 04 and 08.

(K_{ij}), defined as the time rate of change of the displacement covariance, to the integral of the Lagrangian autocovariance. This relation, first derived by Taylor (1921), is expressed as

$$K_{ij}(t) \equiv \frac{1}{2}\frac{d}{dt}\langle d'_i d'_j \rangle = \frac{1}{2}\int_0^t [R_{ij}(\tau) + R_{ji}(\tau)]dt. \qquad (5)$$

Equation (5) approaches two limits independent of the particular form of $R(\tau)$:

1) Initial dispersion

$$\text{if} \quad t \ll T_i^L, \quad \text{then} \quad \frac{1}{2}\frac{d}{dt}\langle d'^2_i \rangle = \langle u'^2_i \rangle t \qquad (6)$$

2) Random walk regime

$$\text{if} \quad t \gg T_i^L, \quad \text{then} \quad \frac{1}{2}\frac{d}{dt}\langle d'^2_i \rangle\langle u'^2_i \rangle T_i^L. \qquad (7)$$

In the second case, the dispersion of particles is governed by the advection–diffusion equation with the diffusivity defined in (5).

In spite of the nonuniform nature of the observations, we begin the analysis with the simplest approach of assumed homogeneity and stationarity and test the above theory of homogeneous turbulence. A large number of independent tracks are necessary to calculate reliable statistics. Since the decorrelation time scale of the individual drifter tracks is less than 10 days (Table 1), any two locations of the same drifter separated in time by more than 10 days are independent and they can be considered as the origins of two independent tracks. Thus, the number of degrees of freedom was increased by considering subtracks whose origins are taken every 10 days along the 25 original trajectories, giving a total of 595 segments. The original and segmented displacement series are plotted versus time after deployment in Fig. 6a. The picture looks like a diffusing plume of dye from a continuous source. It shows the advection and the dispersion of particles by our presumed homogeneous turbulent field. The normalized density of tracks in this displacement-time plane is the probability density $P_1(\mathbf{x}, t; \mathbf{x}_0, t_0)$. Mean and rms displacements are displayed versus time in Fig. 6b. There is good agreement between the mean displacement at each time and the value corresponding to the global mean flow $\langle \mathbf{u} \rangle$ = (−0.5, −3.0) cm s^{-1} calculated from the 595 tracks. This new global mean is compatible with the global mean in section 2; as

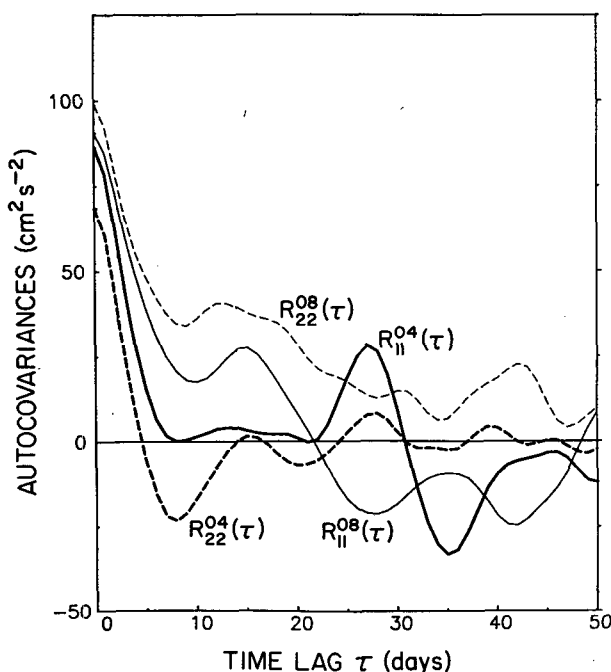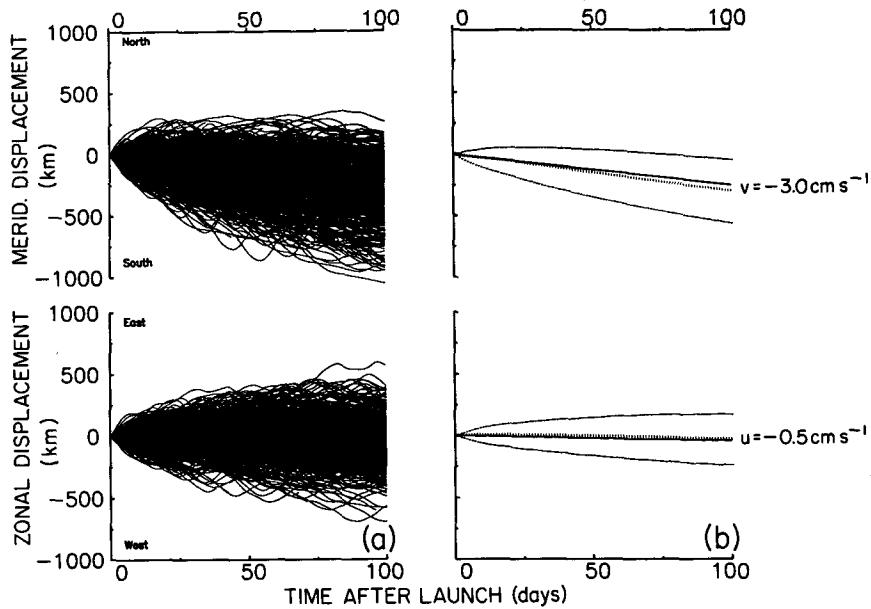FIG. 6. (a) Displacements versus time after deployment for the 595 segmented drifter tracks (see text). (b) Time series of the mean displacements (dots) and associated rms intervals (solid envelopes). The straight solid lines correspond to the global mean velocity $\langle u \rangle = (-0.5, -3.0)$ cm s^{-1}.

expected, there is only a significant southward mean flow of 3–4 cm s^{-1} in the meridional direction.

The new mean was subtracted from the velocities to compute the mean Lagrangian autocovariances (R_{11}, R_{22}) presented in Fig. 7a. The corresponding time-dependent diffusivities are also depicted. The first maxima in the diffusivities and the Lagrangian scales are presented in Table 2. The values appear smaller

than those calculated from individual drifters (Table 1). The different means taken out and the consideration of segmented tracks are the cause of this discrepancy. Energies (autocovariance at zero time lag), scales and diffusivities are numerically larger in the meridional direction. The diffusivities reach stable plateaus after 10 days. Rms displacements are plotted in Fig. 8a for the initial dispersion range. The initial dispersion
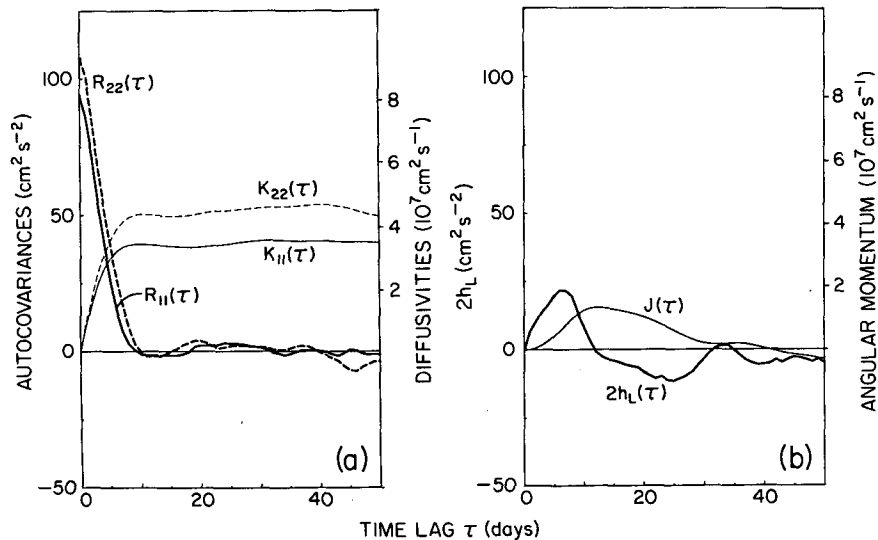

FIG. 7. (a) Mean zonal (solid) and meridional (dashed) Lagrangian autocovariances and diffusivities as a function of time lag. (b) Mean Lagrangian measure of polarization ($2h_L = R_{12} - R_{21}$) and mean angular momentum J versus time lag.

TABLE 2. Velocity variances and Lagrangian scales and diffusivities computed from the 595 drifter tracks.

	Velocity variance $(cm^2\ s^{-2})$		Time scale (days)		Length scale (km)		Diffusivity K $(10^7\ cm^2\ s^{-1})$	
	Zonal	Meridional	Zonal	Meridional	Zonal	Meridional	Zonal	Meridional
595 tracks	94.	108.	4.2	4.7	40.	48.	3.4	4.3

law (6) holds until 2 and 4 days after deployment for the zonal and meridional directions, respectively. The variance of the residual displacements are depicted in Fig. 8b. The two solid lines correspond to the integration of Taylor's theorem (5). In general, the observed dispersions are well modeled by Taylor's theorem.

Higher moments of $P_1(x, t; x_0, t_0)$ were calculated. The skewness $\langle d_i'^3 \rangle$ vanishes in the zonal direction but has significant negative values for meridional displacements. The observed distributions contain more small southward displacements than the pure diffusion model predicts. This is a result of the inhomogeneous dataset in which some of the drifters are moving south very fast, while others drift southward much more slowly. The kurtoses $\langle d_i'^4 \rangle / \langle d_i'^2 \rangle^2$ are not significantly different from 3, the value expected for Gaussian variables.

c. Variability of the diffusivities

It is well known that oceanic diffusivities are non-uniform in space. Horizontal or quasi-horizontal (along isopycnal) diffusivities are known to be connected to the kinetic energy of the mixing eddies. Price (1982), using an extensive SOFAR float dataset (at 700 and 1300 m depth) in the western North Atlantic, showed that the diffusivities are linearly proportional to the velocity variance. The constant of proportionality is the integral time scale

$$K_{ii} = \langle u_i'^2 \rangle T_i^L. \tag{8}$$

On the other hand, Krauss and Böning (1987), in a study of the near-surface eddy field of the North Atlantic with drifters drogued to 100 m depth, showed a linear dependence of the diffusivities on the rms eddy velocity. This relation is possible if one assumes a constant integral length scale of the eddies

$$K_{ii} = [\langle u_i'^2 \rangle]^{1/2} L_i^L. \tag{9}$$

Our extended set of 595 drifter tracks was used to investigate the spatial variations of the diffusivities. Lagrangian scales and diffusivities were computed, using Taylor's theorem (5), from the subset of tracks originating within the squares contoured by a solid line in Fig. 3. The results are plotted versus velocity variance $\langle u_i'^2 \rangle$ in Figs. 9a, b, c. Regression analyses (see Appendix) do not permit an objective discrimination be-

tween (8) and (9). The linear and quadratic fits of diffusivity versus rms eddy velocity are equally good at explaining the observations. The model based on (8) is, however, slightly better (see correlation coefficients in Appendix) and we have plotted the two corresponding regression lines in Fig. 9c. The regression coefficients correspond to the constant time scales $T_1^L = 4.1$ days and $T_2^L = 4.9$ days, similar to the values reported in Table 2.
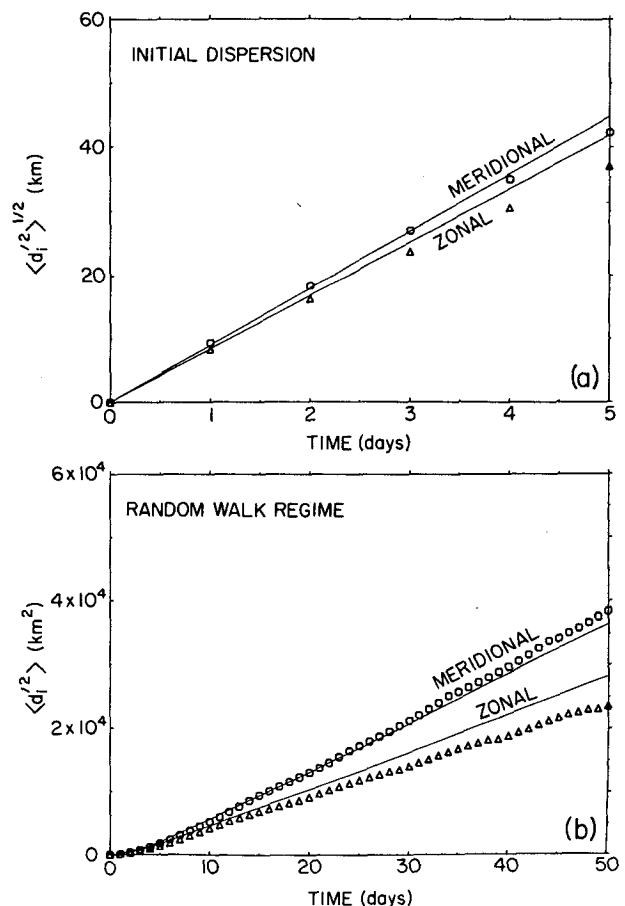

FIG. 8. (a) Initial dispersion regime: Rms displacements versus time; (b) Random walk regime: Displacement variances versus time. Symbols (triangle = zonal, circle = meridional) represent the observations. Taylor's theorem predicts the dispersion depicted by the solid lines.
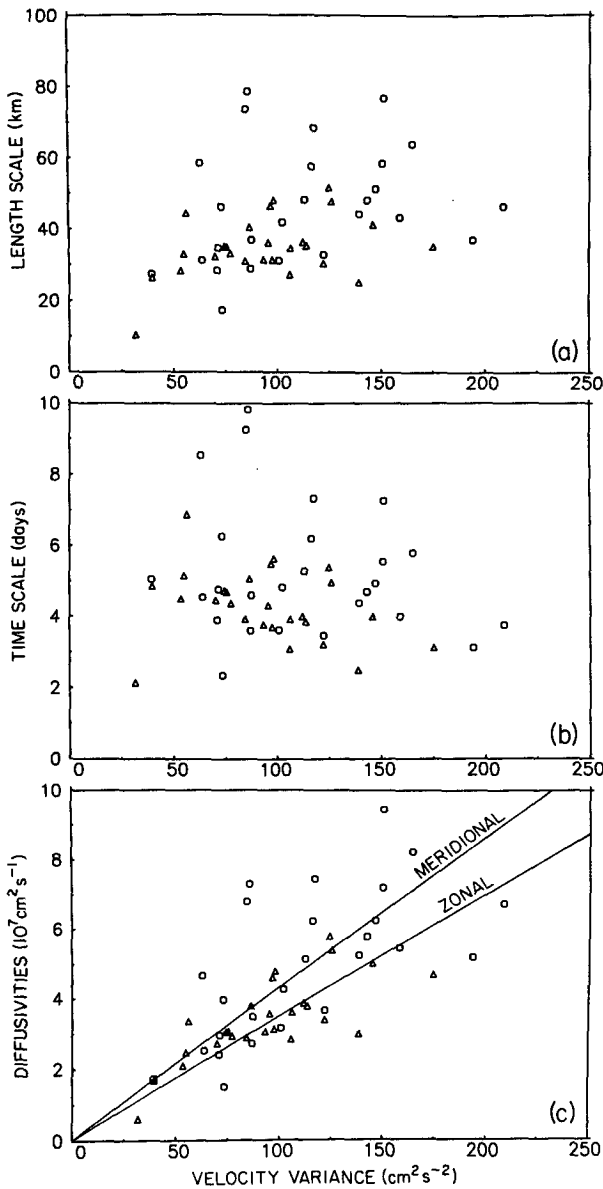
FIG. 9. Lagrangian length (a) and time scales (b) and diffusivities (c) versus velocity variance for the 200×200 km^2 domains contoured by a solid line in Fig. 3. Triangles and circles correspond to the zonal and meridional directions, respectively. The solid lines correspond to the linear regressions presented in the Appendix.

d. Angular momentum of the fluctuations

A Lagrangian measure of polarization or rotation is given by

$$h_L(\tau) = \frac{1}{2} (R_{12} - R_{21}). \tag{10}$$

It is related to the mean angular momentum of the fluctuations

$$J(\tau) = \hat{k} \cdot \langle (x(x_0, t + \tau) - x(x_0, t)) \\ \times u'(x_0, t + \tau) \rangle_L \tag{11}$$

through

$$h_L(\tau) = \frac{1}{2} \frac{\partial J}{\partial \tau}, \tag{12}$$

where $\hat{k}$ is the vertical unit vector and $x(x_0, t)$ is the position at time t of the drifter deployed at x_0. We used the 595 tracks to compute the mean measure of polarization (10). The results (Fig. 7b) show positive values of h_L for time lags less than about two weeks. For larger time lags, h_L is negative. The high positive peak of h_L at about one-week time lag dominates the integration which yields a positive mean angular momentum for time lags less than 40 days. The same computations were made without the large cyclonic eddies (see section 2) and no significant polarization was found. Thus, the Lagrangian measure of rotation (preferential cyclonic) is simply the signature of the large eddies. A careful examination of the drifter tracks (Fig. 1) reveals the presence of both cyclonic and anticyclonic small scale (<50 km) loops and supports our statistical results.

e. Two-particle dispersion

Characteristics of stirring in a property field θ can be developed from multiparticle statistics (Davis 1983). In particular, the evolution of the characteristic scales introduced by stirring or the typical growth of a property cloud's size is easily determined by two-particle separation statistics. Because particles can interact with each other, the dispersion of particles about their center of mass, or, more simply, of one particle with respect to another, is initially different from the absolute dispersion from a fixed origin. It is only when they are separated by a large distance and become independent that their behavior can be described by one-particle statistics and that relative diffusion is equivalent to absolute diffusion.

Let $P_2(x, y, t; x_0, y_0, t_0)$ be the joint probability that two particles released at (x_0, y_0, t_0) reaches (x, y, t). Define the separation probability by integrating over one particle position:

$$P_S(r, t; x_0, y_0, t_0) = \int dx P_2(x, x + r, t; x_0, y_0, t_0), \tag{13}$$

where $r = y - x$ is the separation vector and the integration is over the whole space. If the velocity field is homogeneous and stationary, the separation probability depends only upon r, t and the initial separation vector $r_0 = y_0 - x_0$. The second moment of the separation probability (separation covariance) is

$$\langle r_i' r_j' \rangle(t) = \int dr P_S(r, t; r_0) r_i' r_j', \tag{14}$$
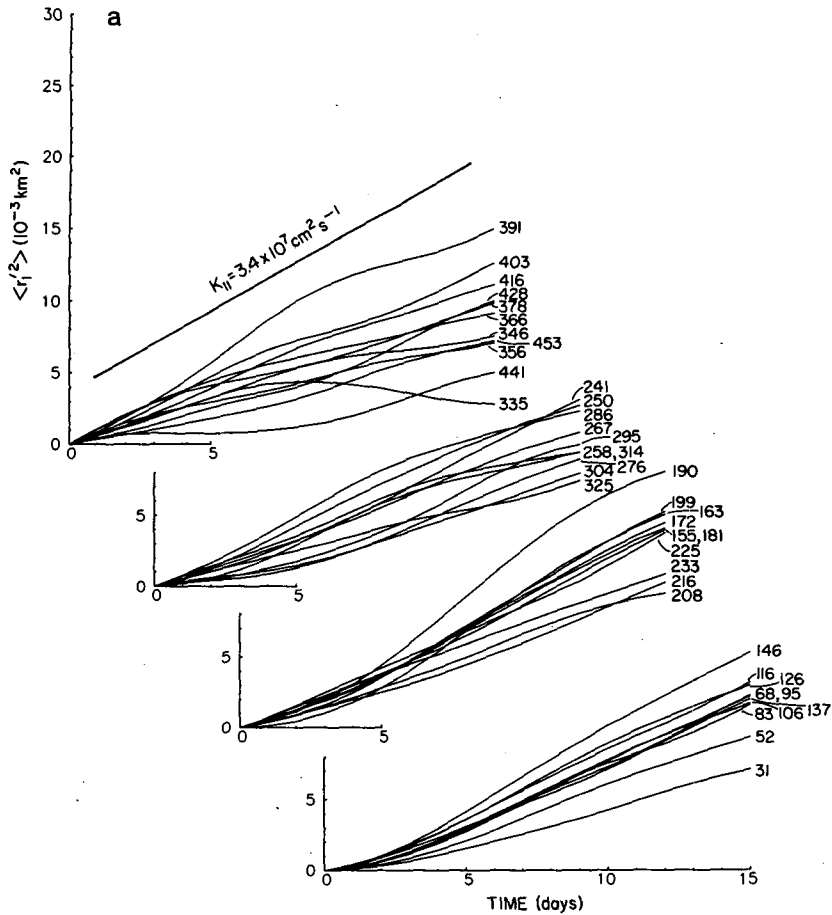
FIG. 10. Zonal (a) and meridional (b) separation variances as a function of time for initial separations between 31 and 453 km. The initial separation is given in kilometers at the end of each curve. The straight lines represent the slopes characteristic of single-particle dispersion.

where $r' = r - \langle r \rangle$ is a residual separation and the integration is over the whole separation space. By analogy with single-particle diffusion, a relative diffusivity is defined as

$$\alpha_{ij}(t, r_0) \equiv \frac{1}{4} \frac{d}{dt} \langle r_i' r_j' \rangle. \tag{15}$$

The dependence on the initial separation vector is expected on the grounds of early observational and theoretical considerations (Richardson 1926; Richardson and Stommel 1948; Stommel 1949). More specifically, relative diffusivity should follow Richardson's $\frac{4}{3}$ power law:

$$\alpha_{ij}(t, r_0) \propto |r_0|^{4/3}. \tag{16}$$

Simply stated, the typical relative velocity of two particles increases as their separation increases. The increase of relative diffusivity with increasing $r_0 = |r_0|$ then follows. For very large r_0, the two particles are independent and the joint probability is separable. As

a consequence, $\langle r_i' r_j' \rangle = 2 \langle d_i' d_j' \rangle$, and the single- and two-particle diffusivities are equal.

Assuming homogeneity and stationarity, the relative diffusivity $\alpha_{ij}(t, r_0)$ was computed from all simultaneous pairs of drifters. The orientation of the initial separation vector appeared to have little influence on the diffusivities. The amplitude of the initial separation vector, r_0, was used to bin the data into classes of 500 pairs. The separation variances $\langle r_i'^2 \rangle$ are plotted versus time in Figs. 10a, b. For small initial separations (<200 km), the zonal separation variances reach a quasi-linear regime after about 5 days and the slopes generally increase with increasing initial separation. For larger initial separation, the behavior of the separation variances is more complicated and slopes can even be negative! In contrast, the evolution of the meridional separation variances with time and initial separation is rather simple: after 5 days of drift, the variances increase quasi-linearly with time and the corresponding slopes increase with increasing initial separation for all the classes considered. Relative diffusivities were com-
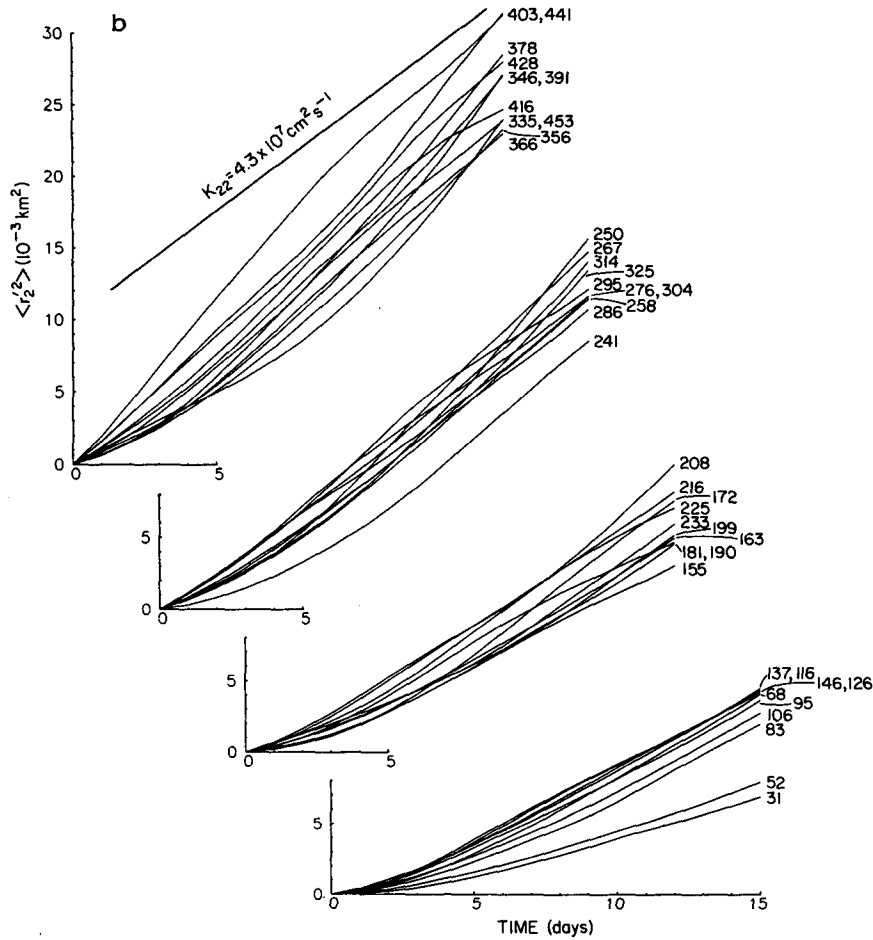
FIG. 10. (*Continued*)

puted from these curves using (15) with 1-day differences. A complex relation between diffusivities, time and rms separation, $\sigma = (\langle r^2 \rangle - \langle r \rangle^2 + \langle r_0 \rangle^2)^{1/2}$, is found (Figs. 11a, b); for each class, the diffusivities increase with time from zero to a saturation value, then decrease or oscillate. Maximum relative diffusivities comparable to the absolute diffusivities ($K_{11} = 3.4 \times 10^7$, $K_{22} = 4.3 \times 10^7$ cm^2 s^{-1}) are obtained for initial separations of about 200 km and 300 km in the zonal and meridional directions respectively. For greater separations, zonal maximum diffusivities decrease and level out at values slightly smaller than K_{11}. In contrast, meridional maximum diffusivities keep increasing and reach values greater than K_{22}. No saturation level seems to be attained for the separation range considered (0–500 km). For small scales (<200 km), diffusivities are essentially isotropic. The scale dependence of the relative diffusivities is illustrated on a log–log plot in Figs. 12a, b. For comparison, the $\frac{4}{3}$ power law (16) is depicted by a straight line.

An attempt was made to describe relative dispersion with a model including horizontal shear and turbu-

lence. Considering pairs of drifters, the relative velocity u_r of one drifter with respect to the other, can be linearly expanded as

$$u_r = \frac{1}{2} (D + N)r_1 + \frac{1}{2} (S - \zeta)r_2 \qquad (17a)$$

$$v_r = \frac{1}{2} (S + \zeta)r_1 + \frac{1}{2} (D - N)r_2, \qquad (17b)$$

where r is the separation vector. Using u_r and r from pairs in different space scale ranges, these equations were solved in the least square sense for the horizontal divergence $D = \partial_x u + \partial_y v$, the vorticity $\zeta = \partial_x v - \partial_y u$ and the shearing and stretching deformation rates $S = \partial_x v + \partial_y u$ and $N = \partial_x u - \partial_y v$. Unfortunately, this shear model was unsuccessful at explaining the variability in the relative velocities. Hence, the flow field observed does not seem to have significant mean divergence, vorticity or deformation rates.

Particle-pair separation histograms were examined for different values of the initial separation r_0. As in
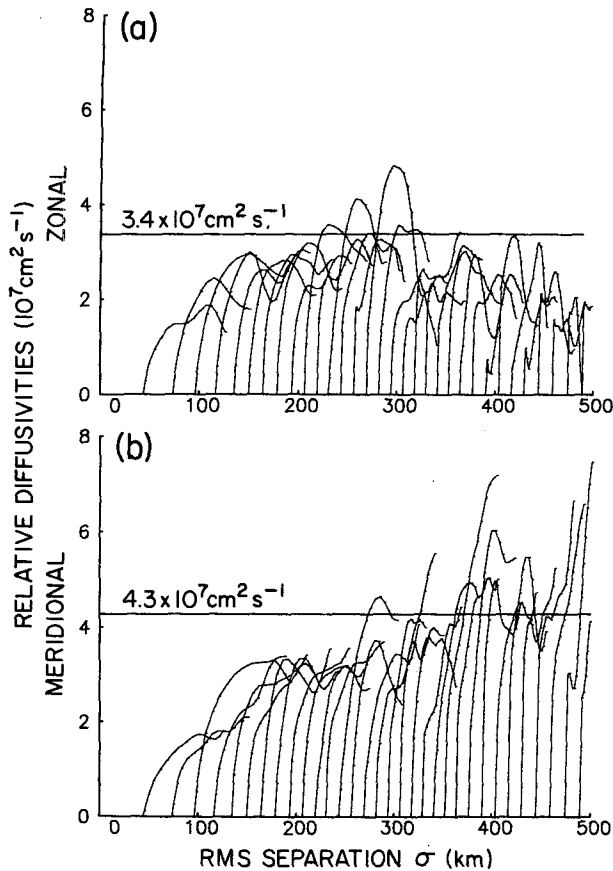
FIG. 11. Relative diffusivities α_{11} (a) and α_{22} (b) as a function of rms separation σ for various initial separations r_0. The time dependence is represented by tick marks plotted daily on each curve.

Davis (1985b), the observed distributions for small r_0 contain more small separations than the distributions corresponding to pure diffusion.

4. Eulerian statistics

We now consider statistics where velocities are considered to be a function of fixed position and time. These Eulerian statistics are discussed from spatio-temporal correlations which are constructed, again, assuming homogeneous and stationary fluctuations.

Consider two velocity observations $\mathbf{v}^1$ and $\mathbf{v}^2$, separated by a displacement vector $\mathbf{r}$ and a time lag τ. Longitudinal and transverse velocity components are defined by $v_L = \hat{\mathbf{r}} \cdot \mathbf{v}$ and $v_T = (\hat{\mathbf{k}} \times \hat{\mathbf{r}}) \cdot \mathbf{v}$ respectively. The following Eulerian correlations are considered:

1) Longitudinal correlation

$$f^{**}(\mathbf{r}, \tau) = \langle v_L^1 v_L^2 \rangle_E$$

$$= \langle v_L(\mathbf{x}, t) v_L(\mathbf{x} + \mathbf{r}, t + \tau) \rangle_E \quad (18a)$$

2) Transverse correlation

$$g^{**}(\mathbf{r}, \tau) = \langle v_T^1 v_T^2 \rangle_E$$

$$= \langle v_T(\mathbf{x}, t) v_T(\mathbf{x} + \mathbf{r}, t + \tau) \rangle_E \quad (18b)$$

3) Mixed correlation

$$h^{**}(\mathbf{r}, \tau) = \frac{1}{2} (\langle v_L^1 v_T^2 \rangle_E - \langle v_T^1 v_L^2 \rangle_E)$$

$$= \frac{1}{2} (\langle v_L(\mathbf{x}, t) v_T(\mathbf{x} + \mathbf{r}, t + \tau) \rangle_E$$

$$- \langle v_T(\mathbf{x}, t) v_L(\mathbf{x} + \mathbf{r}, t + \tau) \rangle_E)$$

$$= \frac{1}{2} (\langle v_1^1 v_2^2 \rangle_E - \langle v_2^1 v_1^2 \rangle_E), \quad (18c)$$

where $\langle \ \rangle_E$ denotes an Eulerian average.

If we can assume isotropy, the general form of the Eulerian correlation tensor can be written as (Middleton and Garrett 1986)
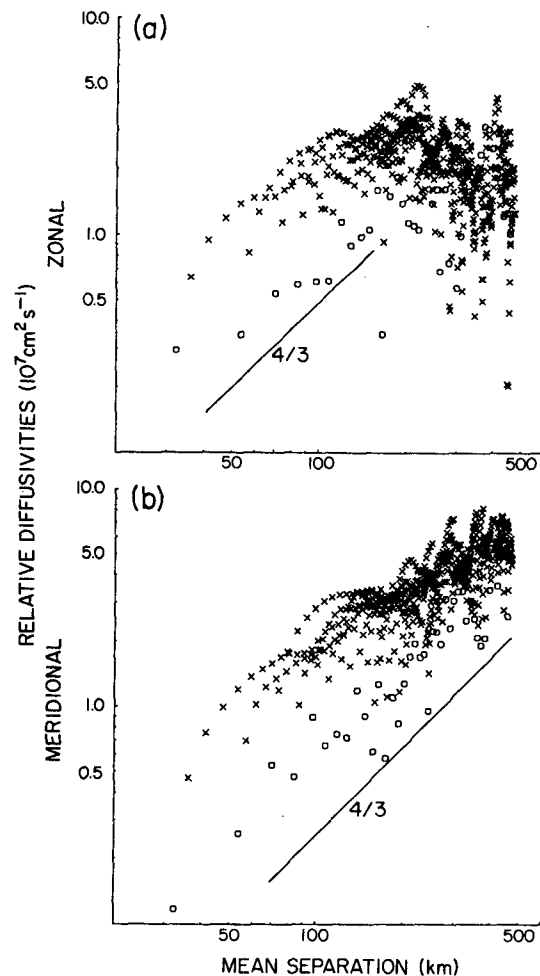

FIG. 12. Zonal (a) and meridional (b) relative diffusivities versus mean separation $\langle r \rangle$ on a log–log plot. Diffusivities after a one day drift are denoted with circles.
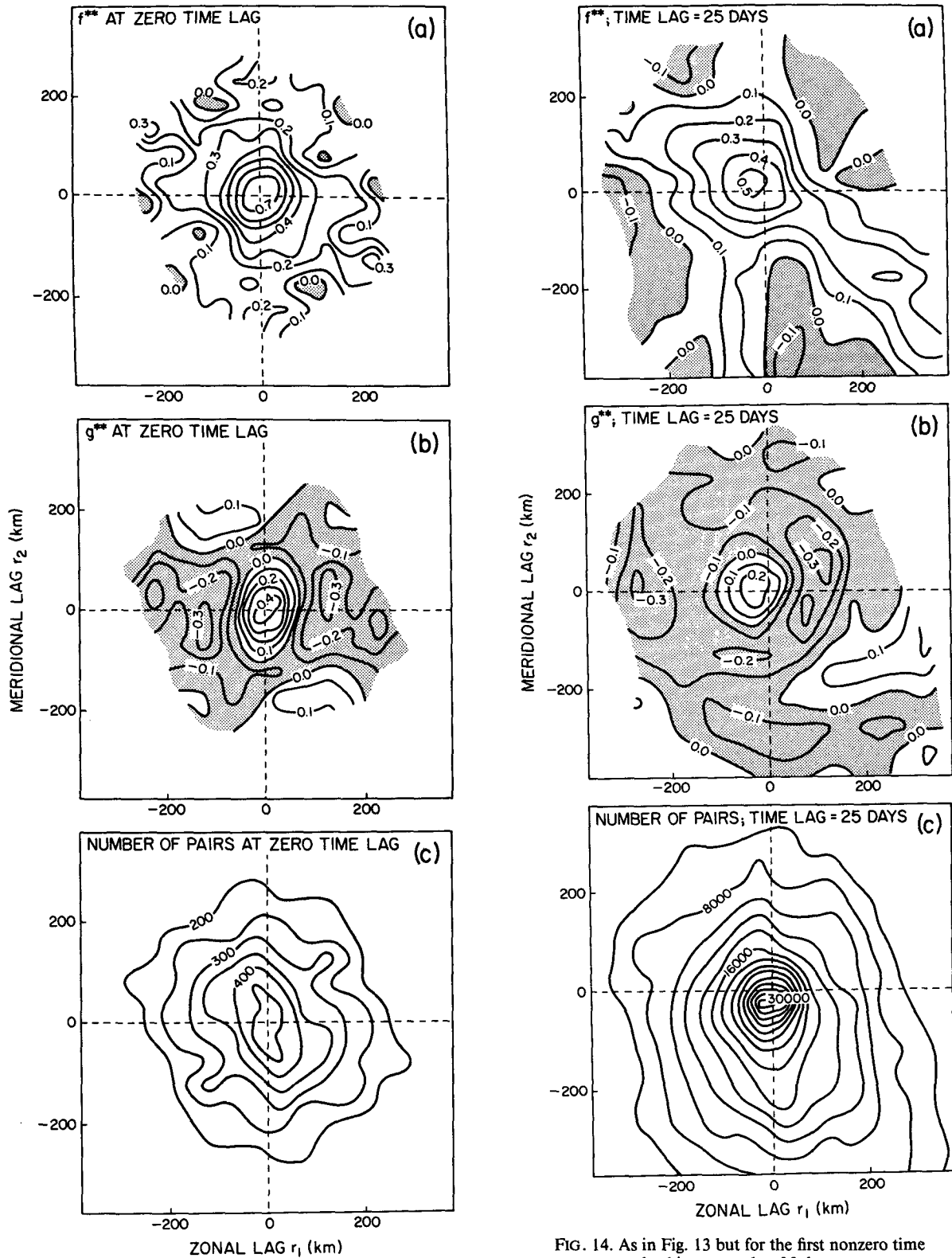
FIG. 13. Eulerian correlation functions for zero time lag: Normalized longitudinal (a) and transverse (b) correlation functions are contoured in the space-lag plane. Regions of negative correlation are stippled. Contour interval is 0.1. The corresponding distribution of number of pairs per bin is depicted in (c).

FIG. 14. As in Fig. 13 but for the first nonzero time lag bin centered at 25 days.

$$\langle v_i(\mathbf{x}, t)v_j(\mathbf{x} + \mathbf{r}, t + \tau)\rangle_E$$

$$= [f^*(r, \tau) - g^*(r, \tau)]r_i r_j/r^2$$

$$+ \delta_{ij} g^*(r, \tau) + \epsilon_{ij} h^*(r, \tau), \quad (19)$$

where $\epsilon_{11} = \epsilon_{22} = 0$, $\epsilon_{12} = -\epsilon_{21} = -1$, δ_{ij} is the Kronecker delta and f^*, g^* and h^* are the isotropic forms of the correlations defined above. The longitudinal and transverse functions are an extension of Batchelor's (1960) f and g functions to include time-lag dependence. The mixed correlation h^* is an odd function of τ which is an Eulerian measure of the preferred sense of rotation at the space and time lags r and τ. It is the Eulerian analog of h_L defined by (12). For positive time lags, h^* is positive for cyclonic eddies.

The global mean velocity, $(0.3, -3.8)$ cm s^{-1}, was first subtracted from all the velocity estimates. Assuming homogeneity and stationarity, the Eulerian ensemble average $\langle \quad \rangle_E$ was replaced by an average in space $(\mathbf{x})$ and time (t). The correlations were computed by accumulating the products within bins in the time and space lags. Bin sizes were chosen in order to obtain reasonably smooth correlation functions and hence, to assure good statistical reliability. Bins of 50×50 km^2 and 50 km $\times$ 50 km $\times$ 50 days were selected for the cases of zero and nonzero time lags respectively. The normalized Eulerian correlations and the number of pairs in bins are depicted for zero time lag in Figs. 13a, b, c. The longitudinal correlation is essentially isotropic. The transverse field shows some anisotropy with the direction of maximum correlation roughly oriented north–south. The distance to the first zero crossing varies from 60 to 100 km. It represents the dominant length scale of the mesoscale field.

We now present the correlation in the first nonzero time bin centered at 25 days. The number of pairs per bin is considerably greater than before (Fig. 14c). The region of the maximum number of pairs extends south in the space-lag plane. This corresponds to the mean California Current in which the drifters are sampling the field while moving equatorward. The maximum correlation, which was at zero spatial lag before, has moved northwest (Fig. 14a). The contours have lost isotropy; there is a tail of positive correlation in the southeast direction. For the transverse correlation (Fig. 14b), we have the same northwestward shift of the maximum; again, any isotropy is lost. This northwestward propagation of the maximum has a speed of about 2 cm s^{-1} and is roughly perpendicular to the mean flow. The same calculations were made with the drifter dataset in which the large cyclonic eddies had been taken out. The results are similar.

Despite some polarization due to the northwestward propagation discussed above, the correlation maps appear nearly isotropic for scales smaller than 200 km. We now assume isotropic fluctuations and compute the Eulerian correlations f^*, g^* and h^*. The normalized f^* and g^* functions at zero time lag and for bins

of 10 km are displayed versus space lag in Fig. 15. The number of pairs per bin is also depicted. The first zero crossing of g^* at about 80 km confirms the previously estimated dominant eddy scale. No negative value is significant for the f^* function. Estimates of h^*, with or without assuming isotropy, are small and noisy. No significant physical result originates from the maps of h^*.

For isotropic turbulence, the Eulerian covariances of the horizontal divergence $D = \partial_x u + \partial_y v$ and vorticity $\zeta = \partial_x v - \partial_y u$ can be expressed as functions of f^* and g^* through (Middleton and Garrett 1986)

$$\langle D(\mathbf{x}, t)D(\mathbf{x} + \mathbf{r}, t + \tau)\rangle_E = \frac{1}{r}\partial_r[g^* - \partial_r(rf^*)]$$

$$(20a)$$

$$\langle \zeta(\mathbf{x}, t)\zeta(\mathbf{x} + \mathbf{r}, t + \tau)\rangle_E = \frac{1}{r}\partial_r[f^* - \partial_r(rg^*)].$$

$$(20b)$$

Since (20a, b) contain second derivatives, smoothed versions (10 first modes of the Fourier transform) of f^* and g^* were used to calculate the divergence and vorticity covariances at zero time lag (Fig. 16). Because of the small number of pairs with very small separation (Fig. 15), the covariances at zero time and space lags, i.e. the mean square divergence $\langle D^2 \rangle_E$ and the mean square vorticity $\langle \zeta^2 \rangle_E$, cannot be directly estimated at small separation with our dataset. For nonzero space lag, however, the covariances show interesting features. The divergence covariance is not significantly different from zero. This means that if the flow field is substantially divergent, the divergence has a very small decorrelation length scale (<10 km). In contrast, the vorticity covariance has values of up to 0.7×10^{-10} s^{-2} for small lags and has a decorrelation length scale of about 50 km. By extrapolation, we estimated an rms vorticity of about 0.8×10^{-5} s^{-1}.
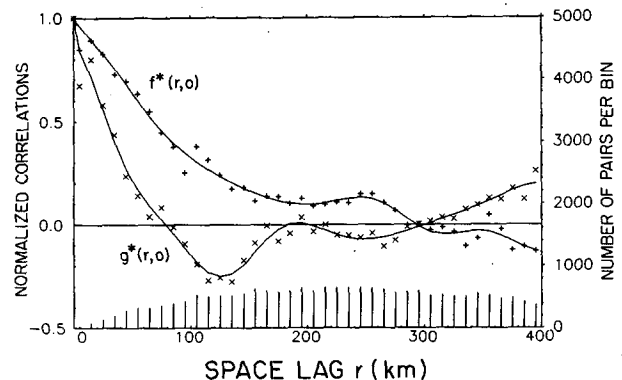

FIG. 15. Isotropic longitudinal $f^*(r, 0)$ and transverse $g^*(r, 0)$ correlation functions for zero time lag as a function of space lag. The solid curves represent the smoothed correlations used in Eqs. (20a, b). The number of pairs per 10-km bin is represented by stick bars at the bottom of the plot.
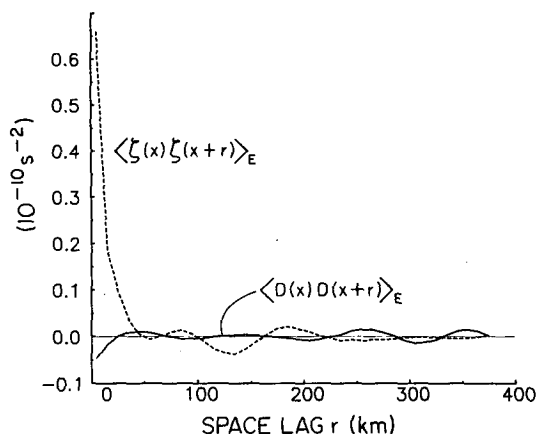
FIG. 16. Divergence (a) and vorticity (b) correlations
as a function of space lag.

5. Discussion and conclusions

Satellite-tracked drifters were used to explore the structure of the surface circulation in the southern California Current System (CCS). The description of flow fields from the trajectories of a limited number of quasi-Lagrangian drifters may give important errors or biases. First, the location calculations by satellite introduce random errors in the velocity estimates. This uncertainty reduces to less than 2 cm s^{-1} for our smoothed velocity time series. Second, the trajectories generally differ from that of the fluid parcel being traced. In our case, the drifter slip with respect to the water is primarily wind-induced and it can be as large as 2 cm s^{-1}. Third, because the observed velocity field also determines the sampling array, substantial biases can be attached to Lagrangian and Eulerian statistics based on a finite number of drifter tracks (see Davis 1985b). For instance, the drifters prefer to sample regions of horizontally convergent motion. In this work, errors due to the limited and Lagrangian natures of the observations were not consistently estimated. Nonetheless, we believe that the results obtained are robust in the sense that they depend drastically neither on the number of observations nor on the particular subsampling adopted.

A glance at the trajectories (Fig. 1) and at the spatial distribution of energy (Fig. 4) indicates that the drifters sampled a very inhomogeneous velocity field. The diversity of the field ranges from almost straight jets to trapping regions or eddies characterized by very different Lagrangian time and space scales. The observed surface circulation has a mean southward drift of 3–4 cm s^{-1} slightly in excess of the slippage error. This represents the weak mean equatorward flow in the CCS. The mesoscale fluctuations about the mean flow have an rms speed of 15 cm s^{-1}.

Despite the obvious nonuniform character of the observations, which is connected to the close proximity

of the coastline and to the localized potential sources of mesoscale variability, we assumed homogeneous and stationary fluctuations to compute Lagrangian and Eulerian statistics. Lagrangian integral time and space scales of 4–5 days and 40–50 km, respectively, were found. This length scale is smaller than the Eulerian decorrelation scale (80 km). Due to the sparsity of the observations within a given region, the Eulerian time scale cannot be estimated. However, we suspect it to be larger than its Lagrangian analog. This agrees with other observations (Davis 1985b; Colin de Verdière 1983; Middleton and Garrett 1986), with numerical simulations (Regier and Stommel 1979) and theoretical considerations (Middleton 1985). Except for large cyclonic eddies, no significant preferential sense of rotation was found in the surface circulation observed.

Absolute and relative dispersions of particles were investigated using single- and two-particle Lagrangian statistics. Taylor's theorem was found to predict the absolute dispersion within the error bars (Fig. 8b). The zonal dispersion, however, appears to be reduced after about 20 days (scale of 100 km), presumably due to the proximity of the coastline. Such a constraint on the dispersion is not present in the Lagrangian velocity autocovariances and, upon integration, Taylor's theory consistently overestimates the observed dispersion. Hence, this discrepancy comes from the nonuniform nature of the dataset. Larger Lagrangian scales and diffusivities are found in the meridional direction; the large meridional diffusivity originates in the coexistence of meridional jets and trapping regions migrating slowly northwest. This result is surprising with regards to simulations of dispersion on the β-plane (Haidvogel and Keffer 1984; Davis 1987) which predicts enhanced dispersion in the zonal direction associated with the propagation of Rossby waves. In our case, the zonal dispersion seems to be limited by other factors such as the proximity of the coast. The anisotropy found in the scales and absolute diffusivities is, however, not statistically significant. We conclude that the dispersion of a passive scalar θ is well modeled by an isotropic advection–diffusion equation for time scale between 5 and 20 days and with a diffusivity of about 4×10^7 cm^2 s^{-1}. For longer time scales, the zonal dispersion is constrained by the coastline and the dispersion becomes anisotropic.

Absolute diffusivities were shown to be linearly proportional to the eddy kinetic energy (Fig. 9c). Our, perhaps subjective, inclination in favor of a constant time scale [and the corresponding relation (8)] means that bigger eddies have stronger circulations. We believe that the reason our dataset follows the same scaling equation (8) as the SOFAR floats is that the rather weak winds encountered in the CCS have little influence on the drifter observations. The drifters provided, therefore, a closer picture of the eddy field near the surface which has statistical characteristics similar to the deeper currents sampled by the SOFAR floats. On

the other hand, the stronger wind regimes of the North Atlantic influence directly (wind slippage) or indirectly (wind-driven circulation) the observations and relation (9) is the result of both the winds and the oceanic eddy field which make up the drifter velocities.

For small initial separation (<200 km), separation variances (Figs. 10a, b) and relative diffusivities (Figs. 11a, b and 12a, b) increase generally with both the magnitude of the initial separation vector and the duration of the drift. The same features were observed by Davis (1985b) closer to the coast off northern California. They are also typical of simulations of particle motions in random velocity fields (Davis 1983). For large initial separation, even though the patterns are more complicated, zonal relative diffusivities saturate and even decrease with increasing initial displacements. This limitation in the relative diffusivity is, again, perhaps a signature of the proximity of the coast. Thus, relative diffusivities are very anisotropic for initial separation larger than 200 km. The best fit with Richardson's $\frac{4}{3}$ power law is for diffusivities after a one day drift (Figs. 12a, b). Unfortunately, after such a short time, we have not reached the linear regime in which a constant diffusivity can be defined. Maximum diffusivities (after 5 days) seem to follow a smaller power ($\approx\frac{1}{2}$) of the separation distance.

The Eulerian correlations at zero time lag were found approximately isotropic for the scales resolved (20–200 km). The Eulerian length scale of the eddy field is 80 km. If a nonzero time lag is introduced, the maximum of both longitudinal and transverse correlations moves northwest at a speed of about 2 cm s^{-1}. This northwestward propagation is not only characteristic of the large cyclonic eddies but also of all other smaller fluctuations. The westward propagation is possibly connected to the tendency of all baroclinic vortices or waves to propagate westward (see also Freeland et al. 1975). It is remarkable, however, that this tendency is not overridden by the mean southward flow. Indeed, if the mesoscale fluctuations were due to local instability of the mean flow, they would propagate to the south within the current. In contrast, eddies propagate roughly normal to this mean. Originally born in the flow, they, perhaps, no longer interact with it and travel westward under the influence of the mean baroclinic vorticity field.

Although our dataset does not permit us to know whether the flow is divergent, we found that if there is substantial divergence, it should have a very small decorrelation length scale (<10 km). Also, Eulerian covariances of vorticity indicate that the motions are rotational with an rms vorticity of 0.8×10^{-5} s^{-1} or 10%–17% of the local f, and a vorticity decorrelation length scale of about 50 km.

APPENDIX

Regression Analyses

The dependence of the Lagrangian decorrelation scales and diffusivities on the velocity variances were analyzed using linear regressions. The variances are expressed in cm^2 s^{-2} and r is the correlation coefficient.

The model based on (8) yields the following regressions

Length scales:

$$L_1^L = 3.62\langle u_1'^2\rangle^{1/2} \text{ km}; \quad r = 0.97$$

$$L_2^L = 4.42\langle u_2'^2\rangle^{1/2} \text{ km}; \quad r = 0.95$$

Time scales:

$$T_1^L = 4.29 \text{ days}; \quad r = 0.97$$

$$T_2^L = 5.26 \text{ days}; \quad r = 0.94$$

Diffusivities:

$$K_{11} = 0.035\langle u_1'^2\rangle 10^7 \text{ cm}^2 \text{ s}^{-1}; \quad r = 0.97$$

$$K_{22} = 0.043\langle u_2'^2\rangle 10^7 \text{ cm}^2 \text{ s}^{-1}; \quad r = 0.95$$

If we consider (9), we have

Length scales:

$$L_1^L = 35.09 \text{ km}; \quad r = 0.97$$

$$L_2^L = 46.76 \text{ km}; \quad r = 0.94$$

Time scales:

$$T_1^L = 37.96\langle u_1'^2\rangle^{-1/2} \text{ days}; \quad r = 0.96$$

$$T_2^L = 51.23\langle u_2'^2\rangle^{-1/2} \text{ days}; \quad r = 0.93$$

Diffusivities:

$$K_{11} = 0.36\langle u_1'^2\rangle^{1/2} 10^7 \text{ cm}^2 \text{ s}^{-1}; \quad r = 0.98$$

$$K_{22} = 0.49\langle u_2'^2\rangle^{1/2} 10^7 \text{ cm}^2 \text{ s}^{-1}; \quad r = 0.95$$

REFERENCES

Batchelor, G. K., 1960: *The Theory of Homogeneous Turbulence.* Cambridge University Press, 197 pp.

Colin de Verdière, A., 1983: Lagrangian eddy statistics from surface drifters in the eastern North Atlantic. *J. Mar. Res.,* **41,** 375–398.

Davis, R. E., 1983: Oceanic property transport, Lagrangian particle statistics, and their prediction. *J. Mar. Res.,* **41,** 163–194.

——, 1985a: Drifter observations of coastal surface currents during CODE: the method and descriptive view. *J. Geophys. Res.,* **90**(C3), 4741–4755.

——, 1985b: Drifter observations of coastal surface currents during CODE: the statistical and dynamical views. *J. Geophys. Res.,* **90**(C3), 4756–4772.

——, 1987: Modeling eddy transport of passive tracers. *J. Mar. Res.,* **45**, 635–666.

Freeland, H. J., P. B. Rhines and T. Rossby, 1975: Statistical observations of the trajectories of neutrally buoyant floats in the North Atlantic. *J. Mar. Res.,* **33**, 383–404.

Haidvogel, D. B., and T. Keffer. 1984: Tracer dispersal by mid-ocean eddies. *Dyn. Atmos. Oceans,* **8**, 1–40.

Haury, L. R., P. M. Poulain, A. W. Mantyla, E. L. Venrick and P. P. Niiler, 1986: FRONTS cruise, data report. SIO Ref. 86-23, Scripps Institution of Oceanography, University of California, San Diego.

Hayward, T. L., A. W. Mantyla and P. P. Niiler, 1987: Physical, chemical and biological data, Cruise SQ86, 15–22 March, 1986. SIO Ref. 87-17, Scripps Institution of Oceanography, University of California, San Diego.

Jennings, F. D., and R. A. Schwartzlose, 1960: Measurements of the California Current in March 1958. *Deep-Sea Res.,* **7**, 42–47.

Krauss, W., and C. W. Böning, 1987: Lagrangian properties of eddy fields in the northern North Atlantic as deduced from satellite-tracked buoys. *J. Mar. Res.,* **45**, 259–291.

McNally, G. J., W. C. Patzert, A. D. Kirwan, Jr. and A. C. Vastano, 1983: The near-surface circulation of the North Pacific using satellite tracked drifting buoys. *J. Geophys. Res.,* **88**(C9), 7507–7518.

Middleton, J. F., 1985: Drifter spectra and diffusivities. *J. Mar. Res.,* **43**, 37–55.

——, and C. Garrett, 1986: A kinematic analysis of polarized eddy fields using drifter data. *J. Geophys. Res.,* **91**(C4), 5094–5102.

Nelson, C. S., 1976: Wind stress and wind stress curl over the California Current. M.S. thesis, Naval Postgraduate School, 136 pp.

Niiler, P. P., R. E. Davis and H. J. White, 1987: Water-following characteristics of a mixed layer drifter. *Deep-Sea Res.,* **34**, 1867–1882.

——, P. M. Poulain and L. R. Haury, 1989: Synoptic three-dimensional circulation in an onshore-flowing filament of the California Current. *Deep-Sea Res.,* **36**, 385–405.

Poulain, P. M., J. D. Illeman and P. P. Niiler, 1987: Drifter observations in the California Current System (1985–1986), data report. SIO Ref. 87-27, Scripps Institution of Oceanography, University of California, San Diego.

Price, J. F., 1982: Particle dispersion in the western North Atlantic. *Eddies in Marine Sciences,* A. R. Robinson, Ed., Springer-Verlag, 609 pp.

Regier, L., and H. Stommel, 1979: Float trajectories in simple kinematic flows. *Proc. Natl. Acad. Sci.,* **76**(10), 4760–4764.

Reid, J. L., 1988: Physical Oceanography, 1947–1987. CalCOFI Rep., XXIX, 42–65.

——, R. A. Schwartzlose and D. M. Brown, 1963: Direct measurements of a small surface eddy off northern Baja California. *J. Mar. Res.,* **21**(3), 205–218.

Richardson, L. F., 1926: Atmospheric diffusion on a distance-neighbor graph. *Proc. Roy. Soc., A.,* **110**, 709–737.

——, and H. Stommel, 1948: Note on eddy diffusion in the sea. *J. Meteor.,* **5**, 238–240.

Schwartzlose, R. A., 1963: Nearshore currents of the western United States and Baja California as measured by drift bottles. California Cooperative Oceanic Fisheries Investigations, Reports, **9**, 15–22.

Stommel, H., 1949: Horizontal diffusion due to oceanic turbulence. *J. Mar. Res.,* **8**(3), 199–225.

Taylor, G. I., 1921: Diffusion by continuous movements. *Proc. London Math. Soc.,* **20**, 196–212.

Tibby, R. B., 1939: Report on returns of drift bottles released off Southern California. *Calif. Fish and Game Fish Bull.,* **55**.